Thermally activated population of microcavity polariton states under optical and electrical excitation

Grant H. Lodden and Russell J. Holmes*

Department of Chemical Engineering and Materials Science, University of Minnesota, Minneapolis, Minnesota 55455, USA

(Received 22 April 2010; revised manuscript received 7 October 2010; published 4 February 2011)

We examine the luminescence from optical microcavities containing an organic semiconductor in the regime of strong exciton-photon coupling. The ratio of luminescence from the upper polariton branch to the lower polariton branch is studied as a function of microcavity detuning and temperature under both optical and electrical excitation. The population of the upper polariton branch is modeled by means of thermal activation from an uncoupled exciton reservoir. Here, the activation energy for the population of the upper polariton branch is equal to the energetic separation between the exciton reservoir and the upper branch at the angle of detection. Agreement is obtained with this model under both optical and electrical excitation using measurements of angle-resolved microcavity reflectivity and luminescence.

DOI: 10.1103/PhysRevB.83.075301 PACS number(s): 78.20.−e, 78.40.Me, 78.55.Kz

I. INTRODUCTION

For a semiconductor embedded in an optical microcavity, a coupling between the resonant photon mode (or cavity mode) and the exciton of the semiconductor occurs when their respective transition energies are degenerate.[1] This coupling can result in two distinct regimes of exciton-photon interaction depending on the relative lifetimes of the exciton and the cavity photon.[2] The relevant temporal figure of merit separating these regimes is known as the Rabi period.[1] When either of the confined cavity photon or exciton decays faster than the Rabi period, the regime of weak exciton-photon coupling is reached. Weak coupling modifies the angular light emission characteristics of the microcavity as well as the linewidth and shape of the emission spectrum.[3,4] If the cavity photon and exciton simultaneously exist for a time longer than the Rabi period, the regime of strong exciton-photon coupling is realized.[1] The eigenfunctions of the strongly coupled system are referred to as microcavity polaritons and are characterized by an energy in-plane wave vector dispersion that splits at the point of degeneracy into two new modes.[1] The size of the splitting in energy and strength of the coupling is quantified by the Rabi splitting $\hbar\Omega$, where Ω is the Rabi frequency.[2] Experimentally, the dispersion is accessed using angle-resolved measurements of reflection, absorption, and luminescence.[5]

Organic semiconductors have received significant interest[6] as active media in strongly coupled devices due to their large exciton binding energies ($\sim$1 eV) (Ref. 7) and oscillator strengths ($\sim 10^{15}$ cm^{-2}).[8] These features have allowed for the observation of strong coupling under both optical and electrical excitation at room temperature.[9–13] Although both photoluminescence (PL) (Refs. 10, 11, and 13–15) and electroluminescence (EL) (Ref. 12) from strongly coupled organic microcavities have been previously reported, the mechanism for the excitation of the polariton branches remains an area of continued research. Of interest is the significant difference in emission intensity between the lower and upper polariton branches observed under optical and electrical excitation.[12,14,16–20] Further, there has been only a single report of EL from strongly coupled organic microcavities, illustrating the need for more investigation into the mechanism for the population of polariton states under electrical excitation.[12]

Since microcavity polaritons are mixed exciton-photon states, their radiative lifetime is a weighted average of the uncoupled exciton and cavity photon lifetimes.[14] As such, the luminescence from microcavity polariton states depends strongly on the degree of exciton-photon mixing. Since the cavity photon lifetime is much shorter than that of the exciton, microcavity polaritons that are photonlike can exhibit more intense luminescence than their excitonlike counterparts. In inorganic semiconductor systems, the emission intensity from the upper and lower polariton branches has a dependence on the detection angle (and hence in-plane wave vector) that reflects the relative degree of photon character.[5,21] In contrast, microcavity polariton emission from organic semiconductor microcavities,[10,12–14] does not correlate with branch photon character. In these systems, emission from the upper polariton branch is many orders of magnitude smaller in intensity than that originating from the lower branch. In order to realize optoelectronic devices based on microcavity polaritons,[22–24] it is important to clearly understand the origin of this discrepancy, and the processes responsible for the population of the upper and lower polariton branches. In this paper, the formation mechanism for microcavity polaritons is elucidated by characterizing PL and EL from microcavities containing the organic semiconductor tetraphenylporphyrin (TPP).[15] The absorption, PL, and EL of TPP are shown in Fig. 1(a). For consistency, the same microcavity structure is characterized using angle-resolved measurements of reflectivity, PL, and EL as a function of both temperature and exciton-photon detuning. This work is a systematic study of the discrepancy in emission intensity from upper and lower branch states under both optical and electrical pumping.

This paper is organized as follows. In Sec. II, the experimental details including device fabrication and various characterization techniques are described. The theoretical basis used to interpret the experimental results is developed in Sec. III, while experimental results are presented in Sec. IV. A discussion of the results is provided in Sec. V, and the conclusions of this work are presented in Sec. VI.

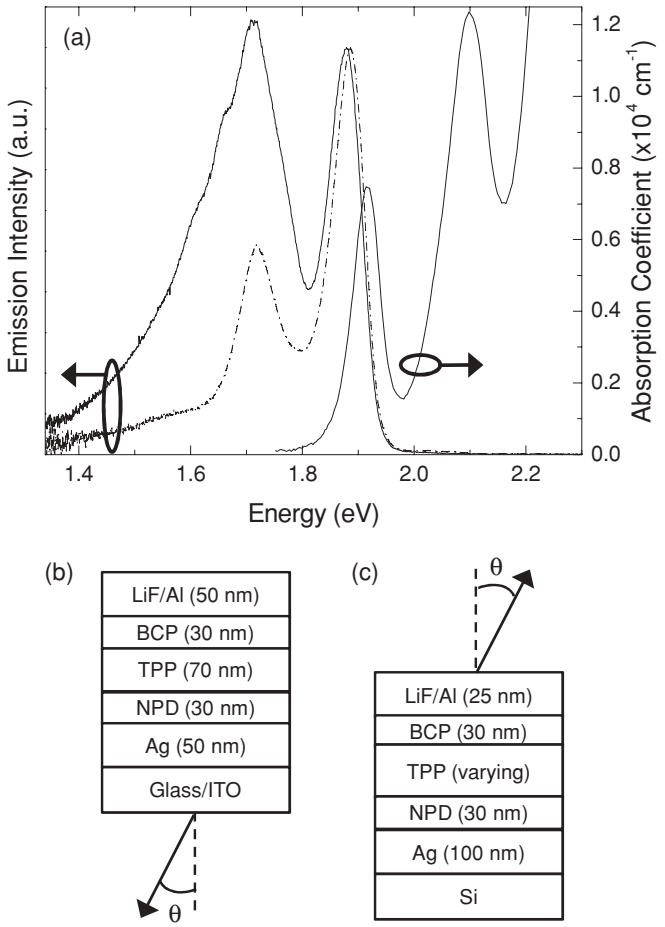

FIG. 1. (a) Absorption coefficient, photoluminescence (PL, broken line), and electroluminescence (EL, solid line) for a 70-nm-thick film of TPP collected at 300 K. The PL spectrum was collected under excitation at a wavelength of 405 nm. The EL spectrum was collected using the bottom-emitting microcavity structure described in Sec. II with the Ag anode omitted. The driving current density was 100 mA/cm^2. Also shown are microcavity architectures for luminescence measurements at (b) room temperature and (c) variable temperature.

II. EXPERIMENT

Two different microcavity architectures were explored in this work to facilitate the measurement of angle-resolved reflectivity, PL, and EL at room temperature [Fig. 1(b)], and measurements of PL and EL as a function of temperature at fixed angle [Fig 1(c)]. In both structures, all device layers were deposited using thermal sublimation at a pressure of $\sim 8 \times 10^{-7}$ Torr. For room-temperature measurements of reflection, PL, and EL, a glass slide coated with a 150-nm-thick layer of indium-tin-oxide (ITO) was used as the substrate. The microcavity [Fig. 1(b)] consisted of a 50-nm-thick layer of Ag, a 30-nm-thick hole-transport layer of *N,N'*-Bis(naphthalen-1-yl) -*N,N'*-bis(phenyl)-benzidine (NPD), a 70-nm-thick layer of TPP, and a 30-nm-thick electron-transport layer of bathocuproine (BCP). The device cathode consisted of a 0.5-nm-thick layer of LiF followed by a 50-nm-thick layer of Al. Here, light is collected through the semitransparent Ag anode.

For temperature-dependent measurements of microcavity luminescence, a polished Si wafer (intrinsic) was used as the substrate to improve thermal coupling to the device active layers. A top-emitting architecture was used to facilitate light extraction for measurements carried out in a cryostat. The device [Fig. 1(c)] consisted of a 100-nm-thick layer of Ag which serves as the anode, a 30-nm-thick layer of NPD, a 55- or 65-nm-thick layer of TPP, a 30-nm-thick layer of BCP, and a cathode consisting of a 0.5-nm-thick layer of LiF followed by a 25-nm-thick layer of Al. Here, light is collected through the semitransparent Al cathode. Due to the change in microcavity architecture, the TPP layer thickness is reduced slightly to permit the study of both the bottom- and top-emitting structures at similar exciton-photon detunings. In each structure, the Ag anode and Al cathode serve both as electrodes and reflectors to form the optical microcavity.[12,25]

Optical microcavities were studied using angle-resolved measurements of reflectivity, PL, and EL. Reflectivity measurements were carried out using a variable-angle spectroscopic ellipsometer under *p*-polarized monochromated white light. Photo- and electroluminescence spectra were collected as a function of angle using an optical fiber-coupled spectrometer. Devices were optically excited using a laser at a wavelength of $\lambda = 405$ nm (60 mW) for PL measurements. For EL measurements, the devices were held at a constant current density of 100 mA/cm^2.

A single port optical cryostat was used for temperature-dependent measurements of PL and EL. For PL measurements, a long-pass filter with a cutoff wavelength of $\lambda = 488$ nm was used to prevent the detection of the pump laser, and the excitation was performed at an angle of 10° from normal. Under both optical and electrical excitation, normal incidence emission spectra were measured as a function of temperature.

III. THEORY

This section outlines a model for the population of upper and lower branch polariton modes that builds off previous work by Ceccarelli *et al.*[16] Here, the emission intensity ratio between the upper and lower branches is modeled under both optical and electrical excitation. Nonresonant excitation of the microcavity leads to the creation of energetic excitons which relax to form an exciton reservoir.[26] Further relaxation from the reservoir can occur by a variety of mechanisms as shown in Fig. 2. Reservoir excitons may undergo radiative or nonradiative decay without coupling (with a total rate of $k_{\mathrm{TOT}} = k_R + k_{NR}$), may form states which are localized and unable to couple,[27] or may couple with the cavity photon mode and populate the upper (k^u) and lower (k^l) branch polariton states. Excitation from the exciton reservoir to the upper polariton branch requires an input of thermal energy. Such phonon-assisted processes are likely facilitated in TPP by the energetic breadth of the uncoupled exciton reservoir.[17,28–31] Since population of the upper branch is a thermally activated process, most reservoir excitons relax into the lower branch.

The polariton formation process described above is modeled using rate equations for the populations of the exciton reservoir (N^r) and the upper and lower polariton branches, N^u

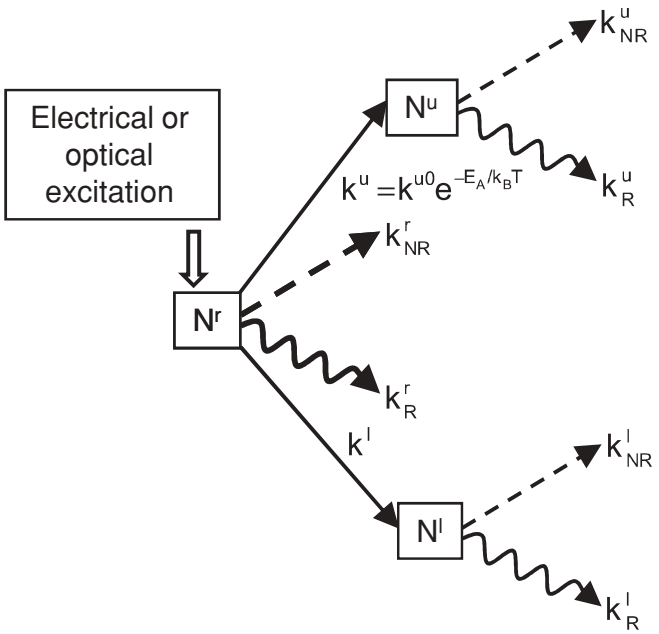

FIG. 2. Exciton relaxation and microcavity polariton formation according to the proposed model. A full explanation of the model is provided in the text.

and N^l, respectively:

$$\frac{dN^r}{dt} = -k^r_{\mathrm{TOT}}N^r - k^l N^r - k^{u0}e^{-E_A/k_BT}N^r + G, \quad (1)$$

$$\frac{dN^u}{dt} = -k^u_{\mathrm{TOT}}N^u + k^{u0}e^{-E_A/k_BT}N^r, \quad (2)$$

$$\frac{dN^l}{dt} = -k^l_{\mathrm{TOT}}N^l + k^l N^r. \quad (3)$$

In Eqs. (1)–(3), k_B is the Boltzmann constant and T is the ambient temperature. Terms referring to the reservoir excitons, upper, and lower branch polaritons are denoted by the superscripts r, u, and l, respectively. The total decay rates for each of the populations are defined as k^r_{TOT}, k^u_{TOT}, and k^l_{TOT}. The rates k^{u0} and k^l are the temperature-independent rates of relaxation and excitation from the reservoir into the upper and lower branches, respectively. The reservoir exciton generation rate (optical or electrical) is G. In this model, polaritons created with arbitrary in-plane wave vector do not undergo further relaxation in energy due to their short radiative lifetime.[14] For high finesse microcavity structures, polaritons may undergo relaxation in the upper and lower branches.[18,19] The upper polariton branch is populated by the excitation of reservoir excitons with activation energy E_A.[16]

Equations (1)–(3) can be solved simultaneously under steady-state excitation to obtain expressions for N^r, N^u, and N^l. The corresponding emission intensity can be expressed as[32]

$$I^j = \frac{\left(k^j_R\right)^2}{k^j_{\mathrm{TOT}}}\frac{d_{\mathrm{Exc}}hc}{\lambda^j}N^j, \quad (4)$$

where h and c are the Planck constant and speed of light, respectively, and the superscript j denotes either r, u, or l. The emission wavelength in each case is denoted by λ^j, and d_{Exc} is the width of the exciton recombination zone. The width of the exciton recombination zone in an organic light-emitting device is typically tens of nanometers.[33,34] Under optical excitation, d_{Exc} can be considerably larger and depends strongly on the absorption coefficient of the organic material. However, when calculating the ratio of luminescence intensities this term cancels, and therefore does not impact the analysis and conclusions drawn from this model. In terms of N^r, the intensities of (4) can be rewritten as

$$I^r = \frac{\left(k^r_R\right)^2}{k^r_{\mathrm{TOT}}}\frac{d_{\mathrm{Exc}}hc}{\lambda^r}N^r, \quad (5)$$

$$I^u = \left(\frac{k^u_R}{k^u_{\mathrm{TOT}}}\right)^2\frac{d_{\mathrm{Exc}}hc}{\lambda^u}k^{u0}e^{-E_A/k_BT}N^r, \quad (6)$$

$$I^l = \left(\frac{k^l_R}{k^l_{\mathrm{TOT}}}\right)^2\frac{d_{\mathrm{Exc}}hc}{\lambda^l}k^l N^r. \quad (7)$$

Using Eqs. (6) and (7), the ratio of upper to lower branch emission can be written as

$$\ln\left(\frac{I^u}{I^l}\right) = \ln(\chi) - \frac{E_A}{k_BT}, \quad (8)$$

where χ depends on the rates of polariton decay and transfer from the reservoir, and the respective emission wavelengths as

$$\chi = \frac{\lambda^l}{\lambda^u}\frac{k^{u0}}{k^l}\left(\frac{k^u_R\left(k^l_R + k^l_{NR}\right)}{k^l_R\left(k^u_R + k^u_{NR}\right)}\right)^2 \quad (9)$$

with[14]

$$k^{u,l}_R \approx \frac{\alpha^2_{u,l}}{\tau_{\mathrm{cav}}}, \quad (10)$$

where α^2 is the relative weight of the photon component of the branch of interest, and τ_{cav} is the photon lifetime in the cavity. Equation (10) reflects the fact that in TPP, τ_{cav} (∼12 fs) is much shorter than the uncoupled exciton lifetime of 0.31 ns.[35] Similarly, the ratio of upper branch emission intensity to reservoir exciton emission intensity can be expressed using Eqs. (5) and (6) as

$$\ln\left(\frac{I^u}{I^r}\right) = \ln(\psi) - \frac{E_A}{k_BT} \quad (11)$$

with

$$\psi = k^{u0}\frac{\lambda^r}{\lambda^u}\left(\frac{k^u_R}{k^r_R}\right)^2\frac{k^r_R + k^r_{NR}}{\left(k^u_R + k^u_{NR}\right)^2}. \quad (12)$$

The emission wavelengths and radiative decay rates for the upper and lower branches [Eq. (10)] can be substituted into Eqs. (9) and (12) to estimate k^l and k^{u0}, the respective rates of polariton population from the reservoir.

IV. RESULTS

A. Microcavity reflectivity at room temperature

The room-temperature thin-film absorption coefficient, PL, and EL of TPP are shown in Fig. 1(a). The optical transition of interest for strong coupling is centered at (1.90 ± 0.02) eV with a full width at half maximum (FWHM) of (61 ± 5) meV.[15,36] In PL and EL, the transitions of interest

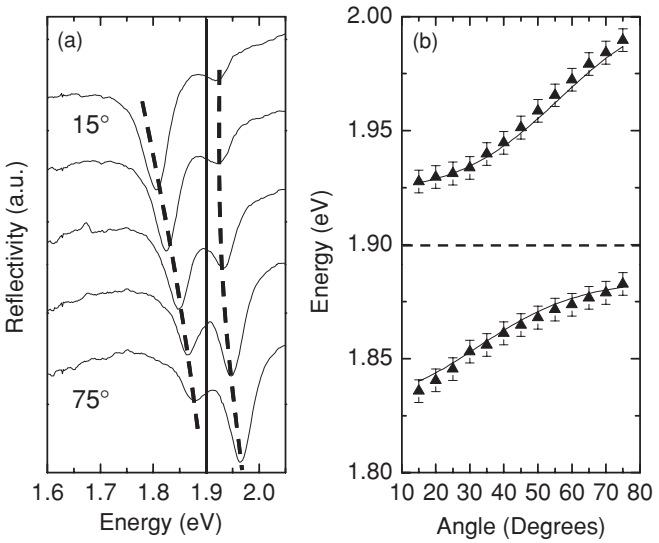

FIG. 3. (a) Reflectivity spectra collected at angles of incidence ranging from 15° to 75° in steps of 15° for the microcavity of Fig. 1(b). The broken lines highlight the dispersion of strongly coupled features with angle. The uncoupled exciton energy is denoted by a solid line. (b) Dispersion relation obtained from reflectivity. Solid lines are fits to the data based on a coupled-oscillator model. The broken line indicates the position of the exciton reservoir.

are centered at (1.89 ± 0.02) eV and (1.88 ± 0.02) eV, with FWHM of (69 ± 5) meV and (68 ± 5) meV, respectively.

Angle-resolved reflectivity spectra for the microcavity structure of Fig. 1(b) are shown in Fig. 3(a). Two prominent features are observed as a result of strong coupling between the cavity photon and the absorption resonance at 1.90 eV. These features show strong dispersion with angle of incidence and anticross around the uncoupled exciton energy.[2] Figure 3(b) shows the corresponding dispersion relation extracted by multipeak fitting the spectra in Fig. 3(a). The dispersion relation was fit using a coupled-oscillator model to yield a Rabi splitting of (80 ± 5) meV.[2]

B. Room-temperature measurements of microcavity luminescence

Figure 4(a) shows angle-resolved PL for the microcavity in Fig. 1(b). Here, a logarithmic plot is used to better resolve emission from the upper polariton branch between 1.90 and 2.05 eV. This feature shows clear dispersion with angle, confirming its origin as the upper polariton branch. Due to the low cavity quality factor ($Q \sim 28$),[32] significant uncoupled emission from TPP is also observed between 1.6 and 1.8 eV. Multipeak fitting (Gaussian) was performed on the emission spectra to extract the position of each feature and construct a dispersion curve [Fig. 4(b)]. As with the

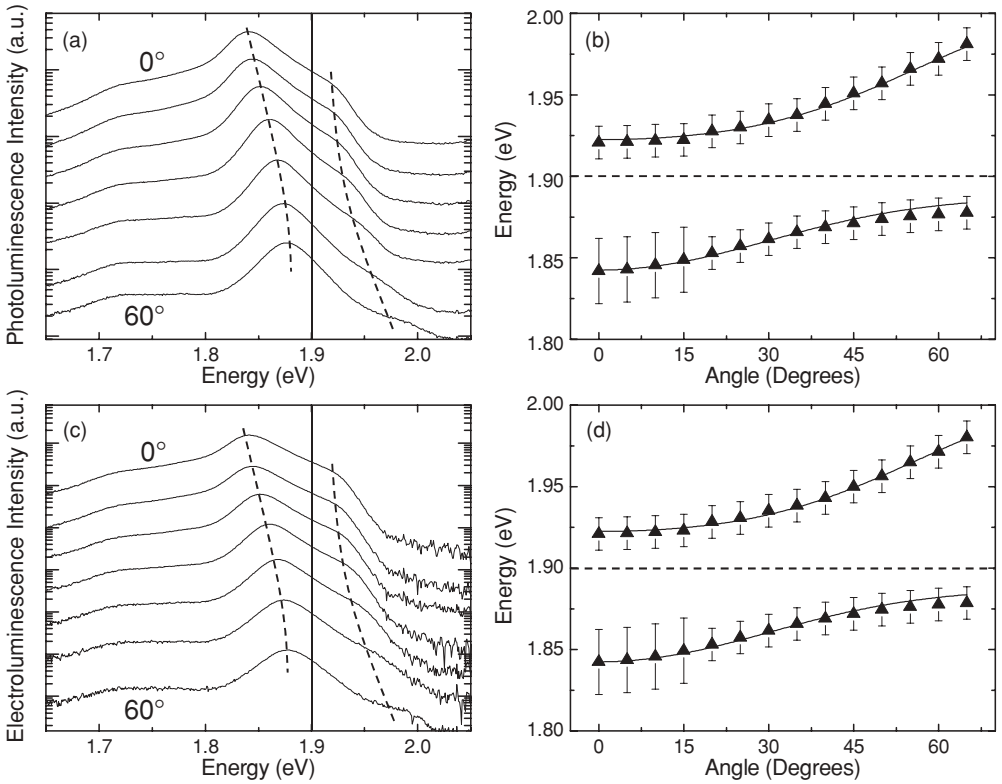

FIG. 4. (a) Logarithmic plot of angle-resolved (steps of 10°) photoluminescence (PL) and (b) the corresponding dispersion relation. (c) Logarithmic plot of angle-resolved (steps of 10°) electroluminescence (EL) and (d) the corresponding dispersion relation. Under both optical and electrical excitation, luminescence is collected for the microcavity of Fig. 1(b). For parts (a) and (c), broken lines indicate the position of the strongly coupled features while the solid lines indicate the position of the uncoupled exciton energy of TPP. For the dispersion relations of parts (b) and (d), solid lines are fits to the data based on a coupled-oscillator model while the uncoupled exciton energy is indicated by a broken line.

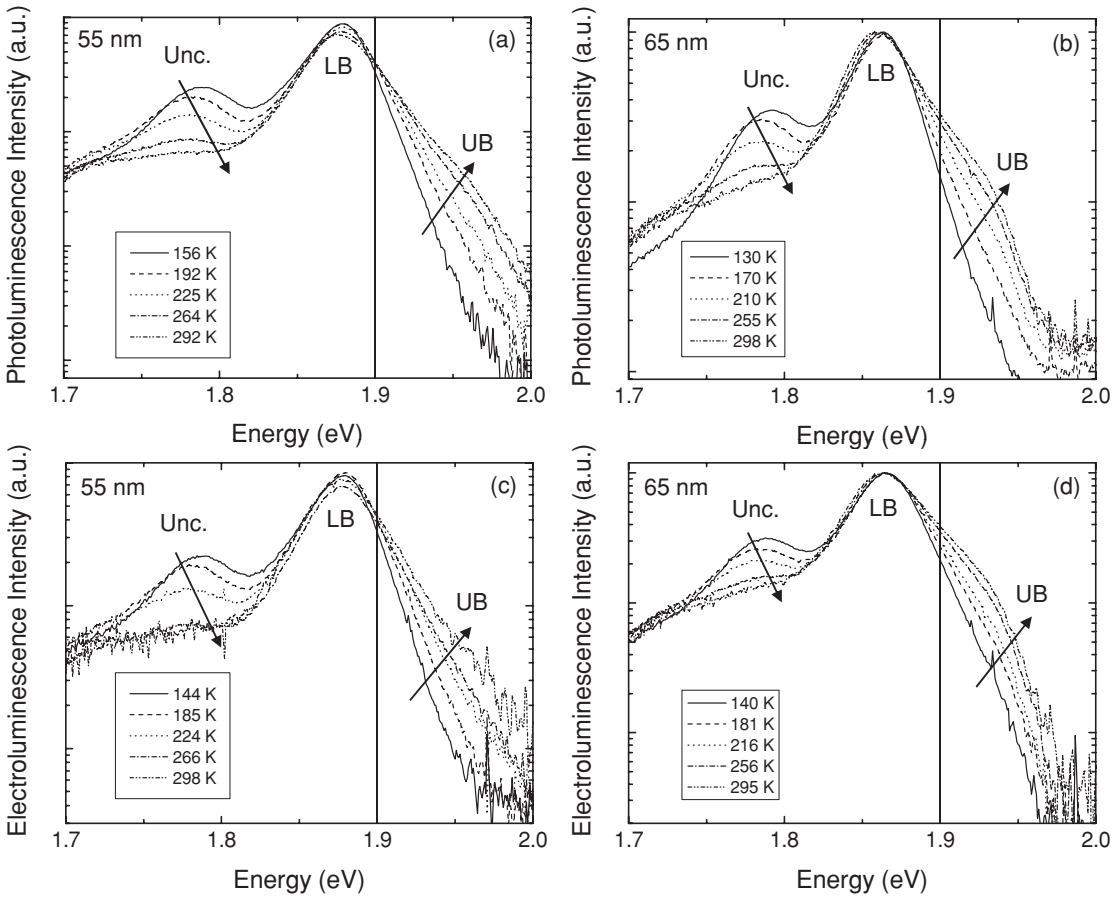

FIG. 5. Photoluminescence (a) and (b) and electroluminescence (c) and (d) spectra collected at normal incidence as a function of temperature for the microcavity of Fig. 1(c). Data for microcavities containing 55 nm of TPP are shown in parts (a) and (c) while data for microcavities containing 65 nm of TPP are shown in parts (b) and (d). The vertical solid line in each figure denotes the position of the uncoupled exciton energy of TPP, while the arrows denote the direction of increasing temperature. The labels Unc., LB, and UB indicate emission from uncoupled reservoir excitons, lower branch polaritons, and upper branch polaritons, respectively.

dispersions obtained from measurements of reflectivity, fitting of the dispersion curve yields a Rabi splitting of (72 ± 5) meV. Angle-resolved microcavity EL spectra are shown in Fig. 4(c), and are similar to those obtained under optical excitation. The corresponding dispersion relation is shown in Fig. 4(d) for the microcavity of Fig. 1(b), characterized by a Rabi splitting of (72 ± 5) meV.

C. Temperature dependence of microcavity luminescence

Microcavity luminescence was also examined as a function of temperature using the top-emitting device architecture described in Sec. II and shown in Fig. 1(c). The PL and EL were collected as a function of temperature for microcavities containing either (55 ± 2) nm or (65 ± 2) nm of TPP. Varying the thickness of TPP changes the cavity mode energy, permitting a variation in the exciton-photon energy detuning. This in turn leads to a variation in the energetic separation between the polariton branches and the exciton reservoir.

Normal incidence PL was collected over a temperature range of 156–292 K [Fig. 5(a)] or 130–298 K [Fig. 5(b)] for devices containing either 55 or 65 nm of TPP, respectively. Similar EL spectra were also collected from microcavities containing either 55 or 65 nm of TPP over a temperature range of 144–298 K [Fig. 5(c)] or 140–295 K [Fig. 5(d)], respectively. The upper and lower polariton branches and

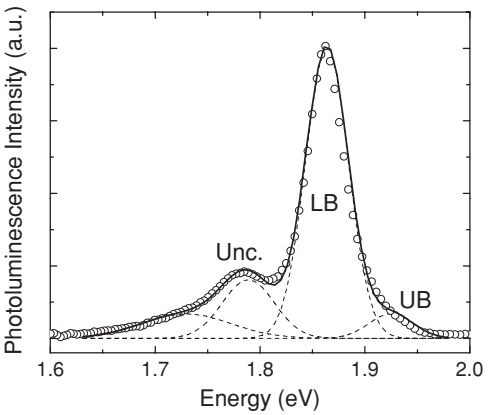

FIG. 6. Multipeak fitting for a photoluminescence spectrum from Fig. 5 collected at 210 K on a device containing 65 nm of TPP (open circles). The spectrum is deconvoluted by multipeak fitting with four Gaussian peaks representing uncoupled emission (Unc., two peaks), lower branch emission (LB), and upper branch emission (UB).

TABLE I. Parameters for temperature-dependent luminescence measurements. The values listed below were determined from fitting the model in Sec. III to the data in Figs. 7 and 8 for microcavities containing either 55 or 65 nm of TPP.

	Photoluminescence			Electroluminescence		
Thickness (nm)	Δ (meV)[a]	E_A (meV)	χ	Δ (meV)[a]	E_A (meV)	χ
55	52 ± 5	52 ± 2	0.50 ± 0.03	56 ± 5	57 ± 2	0.46 ± 0.03
65	28 ± 5	30 ± 2	0.55 ± 0.03	27 ± 5	30 ± 2	0.55 ± 0.03

[a] Δ is the energetic separation between the upper polariton branch and the uncoupled exciton reservoir at an angle of zero degrees.

uncoupled exciton emission are denoted by the labels UB, LB, and Unc., respectively. Significant uncoupled emission is observed as a result of the low microcavity quality factor ($Q \sim 36$).[14,16,37] The spectra in Fig. 5 demonstrate a clear increase in upper branch polariton emission intensity with increasing temperature while the uncoupled emission intensity decreases with increasing temperature, relative to the lower branch.

In order to extract peak positions and intensity from the spectra of Fig. 5, and throughout this work, multipeak fitting (Gaussian) was performed on both PL and EL spectra. Figure 6 shows an example of this deconvolution for a PL spectrum collected at a temperature of 210 K for a microcavity [Fig. 1(c)] containing a 65-nm-thick layer of TPP. The two polariton features are clearly identified along with uncoupled emission from TPP which is best fit using two peaks. Both peak centers and integrated emission intensities were obtained in this way to construct the intensity ratios used for comparison with Eqs. (8) and (11).

Figure 7(a) shows the dependence of the upper branch to lower branch PL ratio on temperature for microcavities [Fig. 1(c)] containing either 55 or 65 nm of TPP. The temperature dependence was fit using (8) to yield activation energies of (52 ± 2) meV and (30 ± 2) meV, and χ values of (0.50 ± 0.03) and (0.55 ± 0.03) for microcavities containing either 55 or 65 nm of TPP, respectively. These parameters are summarized in Table I. The PL intensity of TPP was separately measured outside of the microcavity to have a negligible dependence on temperature. Dispersion relations obtained from angle-resolved reflectivity measurements performed on microcavities containing either 55 or 65 nm of TPP are shown in Figs. 7(b) and 7(c). The dispersion relations were fit with a coupled-oscillator model.

The ratio of the upper branch to lower branch integrated EL intensity was also extracted and plotted as a function of temperature for each detuning [Fig. 8(a)]. Fitting the temperature dependence with (8) yields activation energies of (57 ± 2) meV and (30 ± 2) meV, and χ values of (0.46 ± 0.03) and (0.55 ± 0.03) for microcavities containing either 55 or 65 nm of TPP, respectively. These parameters are summarized in Table I. Dispersion relations obtained from angle-resolved reflectivity are shown for each detuning in Figs. 8(b) and 8(c), and were fit using a coupled-oscillator model.

V. DISCUSSION

A. Exciton-photon coupling at room temperature

The PL and EL spectra shown in Fig. 4 show a significant intensity difference for emission from the lower and upper polariton branches. The lower branch emission intensity correlates well with the photon character of the branch. At angles below resonance, lower branch states are mostly photonlike, and have a shorter radiative lifetime giving rise to efficient emission. At angles above resonance, the emission intensity from lower branch states is reduced due to its excitonlike character and hence longer radiative lifetime. To summarize, lower branch polariton luminescence is more intense at low angles than high angles and emits consistent

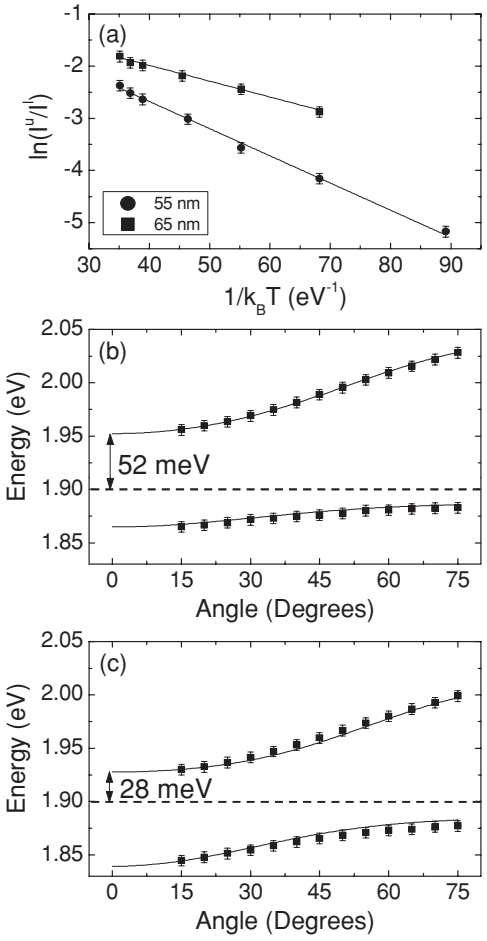

FIG. 7. (a) Temperature-dependent ratio of upper branch to lower branch photoluminescence intensity for the microcavity of Fig. 1(c). Dispersion relations obtained from angle-resolved reflectivity for microcavities containing either (b) 55 nm or (c) 65 nm of TPP. In (b) and (c), the solid lines are fits based on a coupled-oscillator model while broken lines denote the position of the uncoupled exciton reservoir.

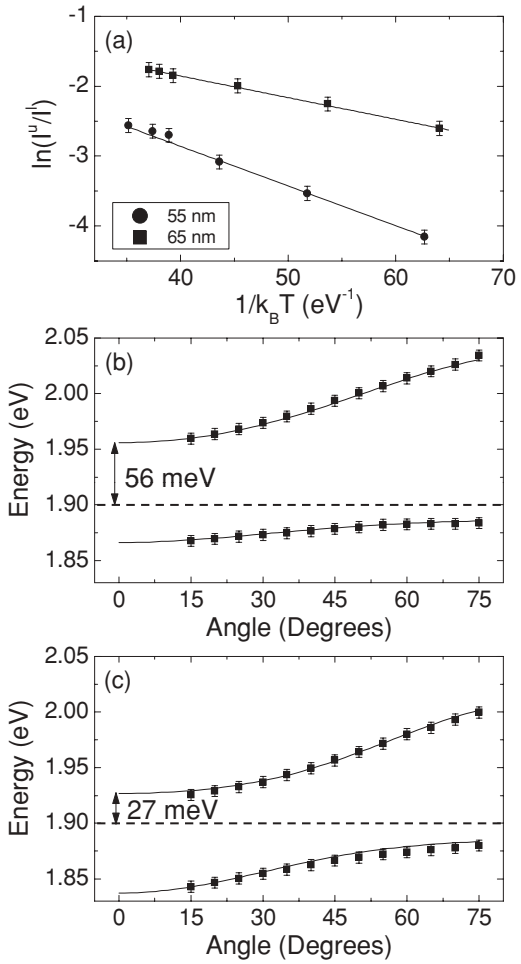

FIG. 8. (a) Temperature-dependent ratios of upper branch to lower branch electroluminescence intensity for the microcavity of Fig. 1(c). Dispersion relations obtained from angle-resolved reflectivity for microcavities containing either (b) 55 nm or (c) 65 nm of TPP. In (b) and (c), the solid lines are fits based on a coupled-oscillator model while broken lines denote the position of the uncoupled exciton reservoir.

with the photon character. This observation is comparable with previous reports of PL from strongly coupled organic microcavities.[12–14] The emission intensity of the upper branch does not exhibit the same dependence on branch character and is instead described using the model of Sec. III.

B. Temperature dependence of microcavity luminescence

1. Activated population of the upper polariton branch

At normal incidence, the energetic separations between the upper branch and the exciton reservoir are (52 ± 5) meV and (28 ± 5) meV for optically excited microcavities containing either 55 or 65 nm of TPP, respectively [Figs. 7(b) and 7(c)]. These values compare favorably with the activation energies of (52 ± 2) meV and (30 ± 2) meV extracted from the fits in Fig. 7(a). Similarly, Figs. 8(b) and 8(c) show dispersion curves obtained from angle-resolved reflectivity for samples examined under electrical excitation. Upper branch-exciton reservoir energetic separations of (56 ± 5) meV and (27 ± 5) meV are observed at normal incidence for microcavities containing 55 or 65 nm of TPP, respectively. These values are in good agreement with the activation energies of (57 ± 2) meV and (30 ± 2) meV extracted from the fits in Fig. 8(a). The correlation between the measured activation energies and the energetic separation between the exciton reservoir and the upper branch (Table I) supports a model of upper branch population via thermal activation. Thus while emission from the lower branch reflects the branch photon character, emission from the upper branch is determined by the rate of population from the exciton reservoir.

2. Population rates of the upper and lower polariton branches

While previous work has examined the ratio of upper to lower branch PL intensity as a function of temperature, there has not been an attempt to extract branch population rates from the temperature dependence of the luminescence.[16] The procedure for extracting the polariton branch population rates is described as follows. First, the intercepts (χ) extracted from fits of Eq. (8) in Figs. 7(a) and 8(a) are manipulated to obtain values for the ratio of the upper branch population rate (k^{u0}) to the lower branch population rate (k^l). Second, the intercepts extracted from fits of Eq. (11) to the ratio of upper branch to reservoir exciton emission intensity (not shown) are used to calculate the upper branch transfer rate k^{u0}, allowing the lower branch excitation rate (k^l) to be extracted from the aforementioned ratio of k^{u0} to k^l.

The vertical-axis intercepts extracted from the fits of Figs. 7(a) and 8(a) can be used to calculate the ratio of k^{u0} to k^l using Eq. (9). This calculation is made under two assumptions, namely that the nonradiative decay rate for lower and upper branch polaritons is the same as that of the uncoupled exciton, and that the nonradiative decay rate is much smaller than the rate of radiative decay from the upper and lower branches. The latter assumption suggests that nonradiative relaxation is not competitive with polariton or reservoir exciton luminescence. The cavity photon lifetime can be calculated from the quality factor yielding a value of 12 fs,[32] allowing the microcavity polariton radiative decay rates to be calculated using Eq. (10). Since both the relaxation rate to the lower branch (k^l) and the rate of transfer from the exciton reservoir to the upper branch (k^{u0}) are unknown, only the ratio of k^{u0} to k^l can be determined from the fits of Fig. 7(a) and 8(a). Substitution into Eq. (9) yields k^{u0} to k^l ratios of (0.44 ± 0.05) and (0.53 ± 0.05), from PL measurements, and (0.48 ± 0.05) and (0.53 ± 0.05), from EL measurements. In both cases the ratios are determined for microcavities containing either 55 or 65 nm of TPP. The ratios of k^{u0} to k^l are summarized in Table II along with their dependence on the energetic separation between the upper branch and the exciton reservoir. Although k^{u0} is defined as the temperature-independent rate of transfer to the upper branch, ratios less than unity suggest that this rate is slower than the relaxation of excitons from the reservoir to the lower branch.

The model developed in Sec. III can be further examined by considering the ratio of upper branch to reservoir emission intensity as a function of temperature. While these data are not included here, they can be fit in analogy to Figs. 7(a)

TABLE II. Polariton excitation rates obtained from the model in Sec. III, and calculated from the fit parameters in Table I as discussed in Sec. V B of the text.

	Photoluminescence		Electroluminescence	
	55-nm TPP	65-nm TPP	55-nm TPP	65-nm TPP
Δ (meV)[a]	52 ± 5	28 ± 5	56 ± 5	27 ± 5
δ (meV)[b]	35 ± 5	61 ± 5	34 ± 5	63 ± 5
k^{u0}/k^{l}	0.44 ± 0.05	0.53 ± 0.05	0.48 ± 0.05	0.53 ± 0.05
k^{u0} (s^{-1})	$(5.2 \pm 0.1) \times 10^{10}$	$(4.7 \pm 0.2) \times 10^{9}$	$(5.6 \pm 0.1) \times 10^{10}$	$(5.2 \pm 0.2) \times 10^{9}$
k^{l} (s^{-1})	$(1.2 \pm 0.1) \times 10^{11}$	$(8.9 \pm 0.9) \times 10^{9}$	$(1.2 \pm 0.1) \times 10^{11}$	$(9.8 \pm 0.9) \times 10^{9}$

[a] Δ is the energetic separation between the upper polariton branch and the uncoupled exciton reservoir at an angle of zero degrees.
[b] δ is the energetic separation between the uncoupled exciton reservoir and the lower polariton branch at an angle of zero degrees.

and 8(a) using Eq. (11). These fits yield activation energies for the population of the upper branch that are identical to those extracted from Figs. 7(a) and 8(a). The corresponding values of the intercept (ψ) are (1.60 ± 0.04) and (1.77 ± 0.04) for microcavities containing 65 nm of TPP for PL and EL, respectively. Values of ψ for microcavities containing 55 nm of TPP are (17.92 ± 0.04) and (19.22 ± 0.04) for PL and EL, respectively. Equation (12) can be used with ψ to calculate a value for the upper branch transfer rate k^{u0}. Assuming that the nonradiative decay rate is small with respect to the radiative rate, k^{u0} can be calculated in terms of the radiative decay rate of uncoupled reservoir excitons in the cavity. The results are $(1.48 \pm 0.05)^{*}k_R^r$ and $(1.64 \pm 0.05)^{*}k_R^r$ from PL and EL measurements on microcavities containing 65 nm of TPP. Based on $k_R = 3.2 \times 10^9$ s^{-1} for TPP,[35] and assuming that $k_R^r \sim k_R$, temperature-independent upper branch excitation rates (k^{u0}) of 4.7×10^9 s^{-1} and 5.2×10^9 s^{-1}, are calculated from measurements of PL and EL, respectively. At 300 K, these values for k^{u0} give overall rates of upper branch excitation (k^{u}) of 1.5×10^9 s^{-1} and 1.6×10^9 s^{-1}. The same method can be used to calculate temperature-independent upper branch excitation rates for a microcavity containing 55 nm of TPP. These rates are summarized in Table II for both microcavities along with the corresponding upper branch-exciton reservoir and lower branch-exciton reservoir energetic separations.

Prior work suggests that the upper branch excitation rate should increase with the energetic separation (Δ) between the upper branch and reservoir for branch energies near the reservoir.[19] For higher energy states in the upper branch, the rate of excitation from the reservoir is expected to decrease with increasing Δ.[19] The experimental results presented here for TPP reflect the behavior expected for low-energy states near the exciton reservoir. In particular, k^{u0} for a microcavity containing a 55-nm-thick layer of TPP is a factor of $\sim$10 larger than that obtained for a microcavity containing a 65-nm-thick layer of TPP (Table II). This is consistent with an increase in Δ for microcavities containing 55 nm of TPP.

Combining the calculated values of k^{u0} with the ratios of k^{u0} to k^{l} previously determined allows the lower branch excitation rate to be estimated as a function of exciton-photon detuning (Table II). Prior theoretical work on strong coupling in organic semiconductors has suggested that the rate of relaxation from the exciton reservoir to the lower branch should decrease as the energetic separation between these states (δ) is increased.[19] The data presented here for microcavities containing TPP show this trend as k^{l} is reduced by a factor of $\sim$10 as the thickness of the TPP layer is increased from 55 to 65 nm (Table II). Increasing the thickness of the TPP layer leads to an increase in δ at normal incidence. Overall, the lower branch transfer rates k^{l} determined in this work for TPP (Table II) are similar to those predicted for microcavities containing *J*-aggregate films.[19,38,39]

VI. CONCLUSION

Previous studies of PL from strongly coupled organic microcavities have shown that luminescence from the upper polariton branch is very weak in intensity relative to that from the lower polariton branch.[16–19] In this work, we examine emission from an organic microcavity under both optical and electrical excitation, and develop a formalism that accurately predicts the difference between the lower branch and upper branch polariton emission intensities. Fitting the temperature-dependent microcavity luminescence intensities yields activation energies that correspond to the energy difference between the upper branch and the reservoir. Using this model, the rates of population of the upper and lower branches from the exciton reservoir are determined. This work may ultimately help to guide the development of alternate excitation schemes which could permit equal population of both polariton branches.[40]

ACKNOWLEDGMENTS

Primary support for this work was received from the University of Minnesota Industrial Partnership for Research in Materials and Interfacial Engineering. Partial support was also received from the NSF MRSEC Program under Awards No. DMR-0212302 and No. DMR-0819885. Part of this work was carried out in the Institute of Technology Characterization Facility, University of Minnesota, which has received capital equipment funding from the NSF through the MRSEC, ERC, and MRI programs. R.J.H. would also like to acknowledge support from 3M through a Non-Tenured Faculty Grant.

*rholmes@umn.edu

[1] C. Weisbuch, M. Nishioka, A. Ishikawa, and Y. Arakawa, Phys. Rev. Lett. **69**, 3314 (1992).

[2] M. S. Skolnick, T. A. Fisher, and D. M. Whittaker, Semicond. Sci. Technol. **13**, 645 (1998).

[3] H. Yokoyama, K. Nishi, T. Anan, H. Yamada, S. D. Brorson, and E. P. Ippen, Appl. Phys. Lett. **57**, 2814 (1990).

[4] R. H. Jordan, L. J. Rothberg, A. Dodabalapur, and R. E. Slusher, Appl. Phys. Lett. **69**, 1997 (1996).

[5] R. Houdre, C. Weisbuch, R. P. Stanley, U. Oesterle, P. Pellandini, and M. Ilegems, Phys. Rev. Lett. **73**, 2043 (1994).

[6] R. J. Holmes and S. R. Forrest, Org. Electron. **8**, 77 (2007).

[7] M. Pope and C. E. Swenberg, *Electronic Processes in Organic Crystals and Polymers* (Oxford University Press, New Yorks, 1999).

[8] D. G. Lidzey, D. D. C. Bradley, M. S. Skolnick, T. Virgili, S. Walker, and D. M. Whittaker, Nature (London) **395**, 53 (1998).

[9] R. J. Holmes and S. R. Forrest, Phys. Rev. Lett. **93**, 186404 (2004).

[10] S. Kena-Cohen and S. R. Forrest, Phys. Rev. B **76**, 075202 (2007).

[11] N. Takada, T. Kamata, and D. D. C. Bradley, Appl. Phys. Lett. **82**, 1812 (2003).

[12] J. R. Tischler, M. S. Bradley, V. Bulovic, J. H. Song, and A. Nurmikko, Phys. Rev. Lett. **95**, 036401 (2005).

[13] D. G. Lidzey, D. D. C. Bradley, T. Virgili, A. Armitage, M. S. Skolnick, and S. Walker, Phys. Rev. Lett. **82**, 3316 (1999).

[14] D. G. Lidzey, A. M. Fox, M. D. Rahn, M. S. Skolnick, V. M. Agranovich, and S. Walker, Phys. Rev. B **65**, 195312 (2002).

[15] R. J. Holmes and S. R. Forrest, Phys. Rev. B **71**, 235203 (2005).

[16] S. Ceccarelli, J. Wenus, M. S. Skolnick, and D. G. Lidzey, Superlattices Microstruct. **41**, 289 (2007).

[17] J. Chovan, I. E. Perakis, S. Ceccarelli, and D. G. Lidzey, Phys. Rev. B **78**, 045320 (2008).

[18] P. Michetti and G. C. La Rocca, Phys. Rev. B **79**, 035325 (2009).

[19] P. Michetti and G. C. La Rocca, Phys. Rev. B **77**, 195301 (2008).

[20] L. Mazza, L. Fontanesi, and G. C. La Rocca, Phys. Rev. B **80**, 235314 (2009).

[21] S. I. Tsintzos, N. T. Pelekanos, G. Konstantinidis, Z. Hatzopoulos, and P. G. Savvidis, Nature (London) **453**, 372 (2008).

[22] S. Kéna-Cohen and S. R. Forrest, Nature Photonics **4**, 371 (2010).

[23] M. Saba, C. Ciuti, J. Bloch, V. Thierry-Mieg, R. Andre, Le Si Dang, S. Kundermann, A. Mura, G. Bongiovanni, J. L. Staehli, and B. Deveaud, Nature (London) **414**, 731 (2001).

[24] P. G. Savvidis, J. J. Baumberg, R. M. Stevenson, M. S. Skolnick, D. M. Whittaker, and J. S. Roberts, Phys. Rev. Lett. **84**, 1547 (2000).

[25] P. A. Hobson, W. L. Barnes, D. G. Lidzey, G. A. Gehring, D. M. Whittaker, M. S. Skolnick, and S. Walker, Appl. Phys. Lett. **81**, 3519 (2002).

[26] N. J. Turro, *Modern Molecular Photochemistry* (University Science Books, Sausalito, CA, 1991).

[27] V. M. Agranovich, M. Litinskaia, and D. G. Lidzey, Phys. Rev. B **67**, 085311 (2003).

[28] S. Pau, G. Bjork, J. Jacobson, H. Cao, and Y. Yamamoto, Phys. Rev. B **51**, 7090 (1995).

[29] S. Pau, H. Cao, J. Jacobson, G. Bjork, Y. Yamamoto, and A. Imamoglu, Phys. Rev. A **54**, R1789 (1996).

[30] S. Pau, J. Jacobson, G. Bjork, and Y. Yamamoto, J. Opt. Soc. Am. B **13**, 1078 (1996).

[31] F. Tassone, C. Piermarocchi, V. Savona, A. Quattropani, and P. Schwendimann, Phys. Rev. B **56**, 7554 (1997).

[32] A. Yariv, *Optical Electronics in Modern Communications* (Oxford University Press, New York, 1997).

[33] N. C. Giebink and S. R. Forrest, Phys. Rev. B **77**, 235215 (2008).

[34] J. Kalinowski, L. C. Palilis, W. H. Kim, and Z. H. Kafafi, J. Appl. Phys. **94**, 7764 (2003).

[35] K. Tanimura, T. Kawai, and T. Sakata, J. Phys. Chem. **83**, 2639 (1979).

[36] D. Dolphin, *The Porphyrins* (Academic, New York, 1978), Vol. 3.

[37] J. R. Tischler, M. S. Bradley, Q. Zhang, T. Atay, A. Nurmikko, and V. Bulovic, Organic Electronics **8**, 94 (2007).

[38] M. Litinskaya, P. Reineker, and V. M. Agranovich, J. Lumin. **119**, 277 (2006).

[39] M. Litinskaya, P. Reineker, and V. M. Agranovich, J. Lumin. **110**, 364 (2004).

[40] G. H. Lodden and R. J. Holmes, Phys. Rev. B **82**, 125317 (2010).